CO impedes superfast O_2 binding in ba_3 cytochrome oxidase from *Thermus thermophilus*

Istvan Szundi[a], Chie Funatogawa[a], James A. Fee[b], Tewfik Soulimane[c], and Ólöf Einarsdóttir[a,1]

[a]Department of Chemistry and Biochemistry, University of California, Santa Cruz, CA 95064; [b]Department of Molecular Biology, The Scripps Institute, MB-8 10550 North Torrey Pines Road, La Jolla, CA 92037; and [c]Chemical and Sciences Department and Materials and Surface Science Institute, University of Limerick, Ireland

Edited* by Harry B. Gray, California Institute of Technology, Pasadena, CA, and approved October 13, 2010 (received for review June 25, 2010)

Kinetic studies of heme-copper terminal oxidases using the CO flow-flash method are potentially compromised by the fate of the photodissociated CO. In this time-resolved optical absorption study, we compared the kinetics of dioxygen reduction by ba_3 cytochrome *c* oxidase from *Thermus thermophilus* in the absence and presence of CO using a photolabile O_2-carrier. A novel double-laser excitation is introduced in which dioxygen is generated by photolyzing the O_2-carrier with a 355 nm laser pulse and the fully reduced CO-bound ba_3 simultaneously with a second 532-nm laser pulse. A kinetic analysis reveals a sequential mechanism in which O_2 binding to heme a_3 at 90 μM O_2 occurs with lifetimes of 9.3 and 110 μs in the absence and presence of CO, respectively, followed by a faster cleavage of the dioxygen bond (4.8 μs), which generates the P intermediate with the concomitant oxidation of heme *b*. The second-order rate constant of 1×10^9 M^{-1} s^{-1} for O_2 binding to ba_3 in the absence of CO is 10 times greater than observed in the presence of CO as well as for the bovine heart enzyme. The O_2 bond cleavage in ba_3 of 4.8 μs is also approximately 10 times faster than in the bovine enzyme. These results suggest important structural differences between the accessibility of O_2 to the active site in ba_3 and the bovine enzyme, and they demonstrate that the photodissociated CO impedes access of dioxygen to the heme a_3 site in ba_3, making the CO flow-flash method inapplicable.

double-laser technique | T. thermophilus ba_3 | oxygen reduction | slow-fast kinetics | O_2 channel

The reduction of dioxygen to water in the heme-copper oxidases takes place at the high-spin heme a_3 and Cu_B heterodinuclear center (for review, see refs. 1 and 2). The reaction has been extensively investigated in several aa_3-oxidases by time-resolved spectroscopic techniques in combination with the CO flow-flash technique (1, 2), in which the reaction is initiated by photolyzing CO bound to heme $a_3{}^{2+}$ in the presence of O_2 (3). The O_2 reduction has commonly been interpreted in terms of a unidirectional sequential mechanism (Scheme 1).

The O_2 reduction in *Thermus thermophilus* ba_3, a B-type oxidase with distant sequence homology to the A-type oxidases (4), has received much less attention (5–7). The enzyme contains the four redox-active metal centers (8–10) and functions as a terminal oxidase for aerobic metabolism under limited oxygen concentration (8–11). It also possesses NO reductase activity (12) suggesting shared evolutionary lineage of O_2/NO reduction in this enzyme. In ba_3, the thermal dissociation of CO from heme $a_3{}^{2+}$ in the dark is significantly faster (0.8 s^{-1}) (5) than in the bovine aa_3 (0.023 s^{-1}) (3, 13), and therefore CO flow-flash experiments on ba_3 require fast mixing; such experiments have recently been reported (6, 7). Moreover, the $Cu_B{}^{+}$-CO complex formed following CO photolysis from heme $a_3{}^{2+}$ in ba_3 decays with a lifetime of approximately 30 ms (14), a rate much slower than that of O_2 binding to heme $a_3{}^{2+}$ in the aa_3-oxidases (approximately 10 μs at 1 mM O_2). This raises the question whether the O_2 binding in ba_3 is compromised by the fate of the photodissociated CO.

In this study, we investigated the reaction kinetics of fully reduced *T. thermophilus* ba_3 with photoproduced O_2 in the absence and presence of CO. Our results show a superfast rate of O_2 binding to heme a_3 in the absence of CO and that the photodissociated CO directly or indirectly impedes dioxygen access to the active site. Both the O_2 binding and O—O bond cleavage rates are 10 times faster in reduced ba_3 than in the reduced bovine enzyme.

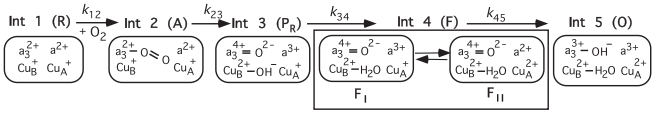

Scheme 1. The conventional sequential unidirectional mechanism for the reduction of dioxygen to water.

Results and Discussion

Time-Resolved Optical Absorption Spectra and Global Exponential Fitting. Fig. 1 *A* and *B* shows the time-resolved difference spectra (post- minus pre-photolysis) recorded during the reaction of fully reduced ba_3 with photoproduced O_2 in the absence and presence of CO, respectively; we will refer to these forms of the enzyme as "ba_3-without-CO" and "ba_3-with-CO." The spectra for the latter were recorded following the simultaneous photolysis of the O_2-carrier with 355 nm light and the fully reduced CO-bound ba_3 with a second 532-nm laser pulse for efficient photolysis. The spectra in the absence and presence of CO are referenced against the spectrum of the reduced enzyme (*A*) and the spectrum of the CO-bound reduced ba_3 (*B*), respectively. Fig. 2 shows a comparison of the O_2 reduction kinetics at 560 and 444 nm for ba_3-with-CO (open and closed circles, respectively) and ba_3-without-CO (open and closed triangles, respectively). It is clear that the early microsecond kinetics of the O_2 reduction are significantly slower for ba_3-with-CO compared to ba_3-without-CO, and the characteristic absorbance changes due to the oxidation and subsequent reduction of heme *b* observed at 560 nm in the absence of CO (open triangles) are much less pronounced in the presence of CO (open circles). The solid and broken lines are the absorbance traces at 560 and 444 nm, respectively, calculated on the basis of the global exponential fits discussed below.

Singular value decomposition (SVD)-based global exponential fitting (15–18) resolved four apparent lifetimes (τ), 4.8 μs, 9.3 μs, 55 μs, and 1.0 ms, for ba_3-without-CO (Fig. S1). Three apparent lifetimes, 59 μs, 110 μs, and 0.82 ms, were obtained for ba_3-with-CO with no early microsecond lifetimes being observed.

Author contributions: I.S., J.A.F., C.F., and O.E. designed research; I.S. and C.F. performed research; I.S. analyzed data; J.A.F. and T.S. contributed new reagents/analytic tools; and I.S. and O.E. wrote the paper.

The authors declare no conflict of interest.

*This Direct Submission article had a prearranged editor.

[1]To whom correspondence should be addressed. E-mail: olof@chemistry.ucsc.edu.

This article contains supporting information online at www.pnas.org/lookup/suppl/doi:10.1073/pnas.1008603107/-/DCSupplemental.

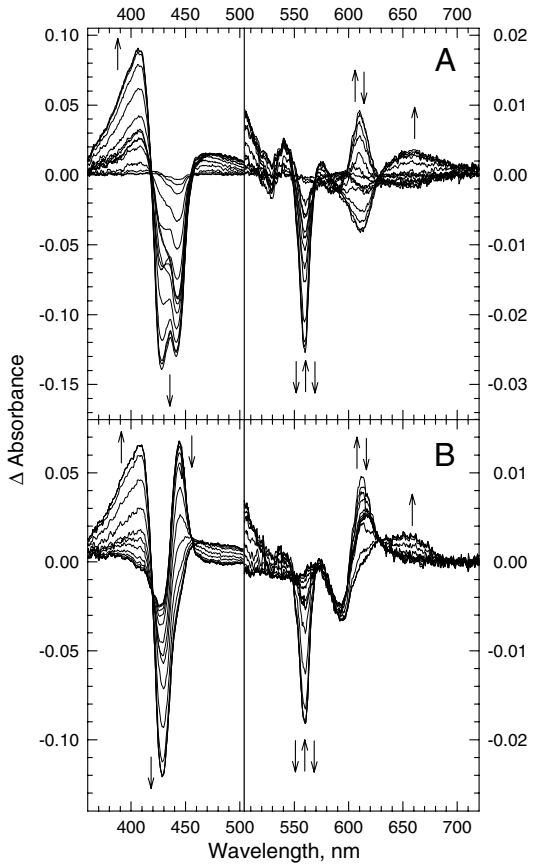

Fig. 1. Time-resolved optical absorption difference spectra (post-minus pre-photolysis) recorded during the reaction of the fully reduced ba_3 with dioxygen in the absence of CO (*A*) and the presence of CO (*B*). The spectra are those obtained after subtracting the spectral contribution of the O_2 complex, determined in a separate experiment. The spectra (SVD-filtered) were recorded at 15 delay times, equally spaced on a logarithmic scale, between 500 ns and 20 ms. The arrows (left to right) represent the direction of the absorbance change with time. Conditions: 0.1 M HEPES (pH 7.5), 0.1% DM; effective enzyme concentration: 2.6 μM (*A*) and 2.0 μM (*B*); optical path, 0.5 cm.

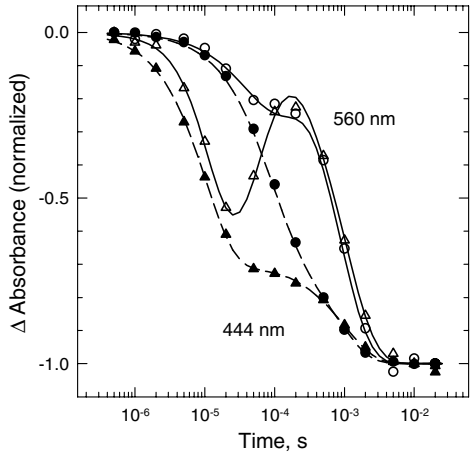

Fig. 2. Comparison of the transient absorbance changes taking place during the reduction of dioxygen to water in ba_3 at 560 nm and 444 nm in the presence of CO (open and closed circles, respectively) and in the absence of CO (open and closed triangles, respectively). The kinetic traces are from the time-resolved data in Fig. 1 and are normalized to the total absorbance change. The solid and broken lines represent the absorbance traces at 560 and 444 nm, respectively, calculated on the basis of the global exponential fits (see text for details).

$$\text{Int 1} \xrightarrow{4.8\ \mu s} \text{Int 2} \xrightarrow{9.3\ \mu s} \text{Int 3} \xrightarrow{55\ \mu s} \text{Int 4} \xrightarrow{1.0\ ms} \text{Int 5}$$

Scheme 2. The conventional unidirectional sequential mechanism of O_2 reduction for ba_3-without-CO.

Kinetic Analysis Based upon the Conventional Unidirectional Sequential Mechanism. The apparent lifetimes and the associated spectral changes, the *b*-spectra (Fig. S2), obtained in the global exponential fitting do not represent real physical processes or different phases of a reaction sequence. Rather, they reflect the fact that all the steps involved in the mechanism are first-order or pseudo-first-order reactions. It is the proposed mechanism that connects the apparent rates to the microscopic rates and the *b*-spectra to the spectra of the intermediates in a real physical mechanism (17, 18). The simplest and mathematically defined mechanism is the conventional unidirectional sequential mechanism in which the experimental apparent rate constants are assigned to microscopic rate constants of the consecutive steps. We first analyzed the ba_3-without-CO data using a five-intermediate unidirectional sequential mechanism (Scheme 2). Because only three lifetimes (four intermediates) were obtained for ba_3-with-CO, we first calculated its experimental intermediate spectra on the basis of a four-intermediate unidirectional sequential mechanism (Scheme 3).

Fig. 3 shows the experimental intermediate spectra for ba_3-without-CO (*A*) and ba_3-with-CO (*B*) calculated for Schemes 2 and 3, respectively. For easier comparison, the datasets are normalized to the concentration of ba_3-with-CO, and both are referenced versus the reduced enzyme, **R**. The spectrum of Int 2 for ba_3-without-CO (Fig. 3*A*, green curve) has no equivalent in the spectra for ba_3-with-CO. Importantly, this spectrum has the same shape as that of compound **A**, observed for the reduced bovine aa_3 using the traditional CO flow-flash method (19) but with a significantly smaller amplitude (approximately 50%); similar amplitude discrepancy was also noted in a recent fast-mixing CO flow-flash experiment on ba_3 (6). The spectrum of Int 3 for ba_3-without-CO (Fig. 3*A*, red curve) is well modeled by the heme a_3 spectrum of **P** (referenced versus the reduced heme a_3) and the oxidized-minus-reduced spectrum of heme *b* (Fig. S3) and will be referred to as $\mathbf{P_I}$. The spectrum of Int 2 for ba_3-with-CO (Fig. 3*B*, red curve) has very similar shape to that of Int 3 for ba_3-without-CO (Fig. 3*A*, red curve) but smaller amplitude. The origin of this amplitude difference and that of Int 2 for ba_3-without-CO and the model compound **A** spectrum will be discussed in detail below. The observed spectral shape and amplitude of Int 4 for ba_3-without-CO (Fig. 3*A*, cyan) were found to be in good agreement with those of Int 3 for ba_3-with-CO (Fig. 3*B*, cyan). These spectra represent **P** with reduced heme *b*; we designate this intermediate as $\mathbf{P_{II}}$. Similarly, good agreement is observed between the final intermediates (the oxidized enzyme) in the absence of CO (Fig. 3*A*, magenta) and presence of CO (Fig. 3*B*, magenta). While the spectra of the last two intermediates in the absence and presence of CO are in agreement and consistent with expected model spectra of the respective intermediates, the amplitude of Int 2 calculated from the ba_3-without-CO data using Scheme 2 is significantly smaller than that of the bovine compound **A** model spectrum. There is no physical reason that would justify such a large amplitude difference, and therefore we must conclude that the traditional unidirectional sequential scheme does not describe the experimental data.

$$\text{Int 1} \xrightarrow{59\ \mu s} \text{Int 2} \xrightarrow{110\ \mu s} \text{Int 3} \xrightarrow{0.82\ ms} \text{Int 4}$$

Scheme 3. A four-intermediate unidirectional sequential mechanism of O_2 reduction for ba_3-with-CO.

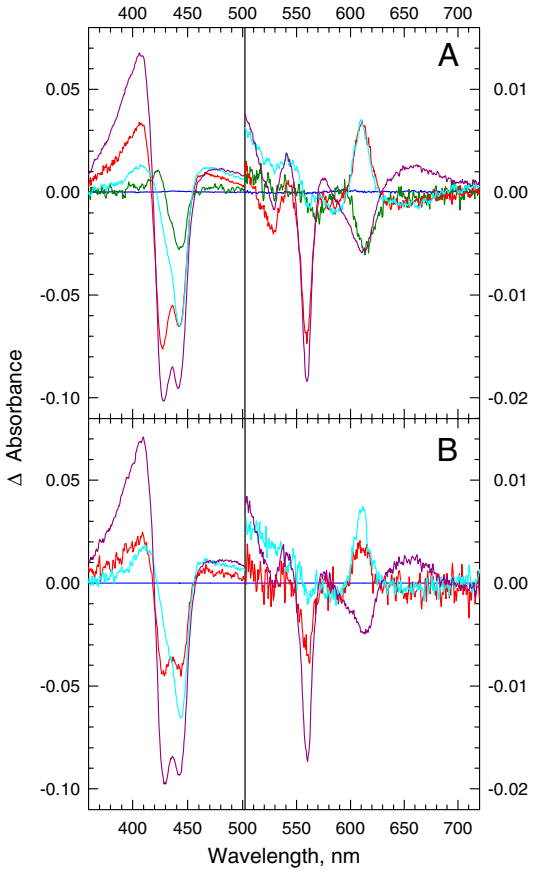

Fig. 3. The experimental intermediate spectra for the reaction of reduced ba_3-without-CO (*A*) and ba_3-with-CO (*B*) with dioxygen, extracted on the basis of Schemes 2 and 3, respectively. The spectra in *A* are normalized to the enzyme concentration in *B*. The intermediate spectra are referenced versus the reduced enzyme. *A* (green) Int 2, (red) Int 3, (cyan) Int 4 and (magenta) Int 5 of Scheme 2; the spectrum of Int 2 has the shape of compound **A** of the bovine heart oxidase but significantly lower amplitude. *B* (red) Int 2, (cyan) Int 3 and (magenta) Int 4 of Scheme 3.

Analysis of the ba_3-Without-CO Data Using a Reversible O_2-Binding Scheme. The most obvious explanation for the reduced amplitude of Int 2 in Scheme 2 and the one proposed in a recent CO flow-flash study on ba_3 (6) is that the O_2 binding is reversible in ba_3. This mechanism is represented in Scheme 4. It should be noted that having only four experimental apparent rates and five microscopic rates in Scheme 4, the spectra of the intermediates can no longer be calculated directly. However, they can be obtained for a presumed degree of reversibility using the algebraic kinetic analysis method outlined below.

The first step in describing a reversible mechanism is constructing the kinetic matrix containing the microscopic rate constants and deriving its eigenvalues, λ_i (see *SI Text* for a detailed analysis). The eigenvalues with the sign reversed are the apparent rate constants r_i, which are the inverse of the apparent lifetimes $\tau_i (r_i = 1/\tau_i)$. The last two apparent rates, r_3 and r_4, are equal to the microscopic rates of the last two steps, k_{34} and k_{45} in Scheme 4, respectively. By introducing the equilibrium constant, $Q = k_{12}/k_{21}$, we can relate the microscopic rate constants, k_{12}, k_{21}, and

$$\text{Int 1 } (\mathbf{R}) \underset{k_{21}}{\overset{k_{12}}{\rightleftarrows}} \text{Int 2 } (\mathbf{A}) \overset{k_{23}}{\rightarrow} \text{Int 3 } (\mathbf{P_I}) \overset{k_{34}}{\rightarrow} \text{Int 4 } (\mathbf{P_{II}}) \overset{k_{45}}{\rightarrow} \text{Int 5 } (\mathbf{O})$$

Scheme 4. The sequential scheme involving a reversible first step (O_2 binding) during the reaction of ba_3 with photoproduced O_2 in the absence of CO. Note that k_{12} is a pseudo-first-order rate constant: $k_{12} = k[O_2]$.

k_{23}, to the first and second apparent rates, r_1 and r_2, and express them as a function of Q (see *SI Text* for a detailed analysis):

$$k_{12} = r_1 r_2 / k_{23}, \quad [1]$$

$$k_{21} = r_1 r_2 / k_{23} Q, \quad [2]$$

$$k_{23} = \{r_1 + r_2 \pm [(r_1 + r_2)^2 - 4 r_1 r_2 (1 + 1/Q)]^{1/2}\}/2. \quad [3]$$

Considering only real number solutions for k_{23} places the following limits on Q:

$$Q \geq 4 r_1 r_2 / (r_1 - r_2)^2 \quad \text{thus}$$
$$Q_{\min} = 4 r_1 r_2 / (r_1 - r_2)^2 = 4 \tau_1 \tau_2 / (\tau_2 - \tau_1)^2. \quad [4]$$

This interesting and unexpected result means that the degree of reversibility cannot be set to any arbitrary value. Instead, its range is restricted by the values of the apparent lifetimes, and the closer in value they are, the narrower this range becomes. In the final step of the analysis, the intermediate spectra were obtained from the experimental *b*-spectra (b_{exp}) and the eigenvectors ($\mathbf{W}_{rev}$) of the kinetic matrix constructed from the microscopic rates (18):

$$\text{Int}_{rev} = b_{exp} \times \mathbf{W}_{rev}{}^{-1}. \quad [5]$$

The above kinetic analysis was applied to ba_3-without-CO. From the two shortest apparent lifetimes, 4.8 μs and 9.3 μs, we calculated a minimum value for the equilibrium constant, $Q_{\min} = k_{12}/k_{21} = 7.8$, which indicates that the binding of O_2 to reduced ba_3 is practically irreversible. As Eq. **3** predicts and is shown in Fig. 4*A*, there are two values for each of the microscopic rates, k_{12}, k_{21}, and k_{23}, at every $Q > Q_{\min}$. The dashed lines represent the case in which k_{23} (circles) decreases and k_{12} (triangles) increases, approaching r_2 and r_1 at $Q = \infty$, respectively, a situation reflecting the traditional mechanism in which the fastest process comes first. The solid lines represent the slow-to-fast order of the kinetic steps in which k_{23} increases and reaches r_1 at $Q = \infty$ while k_{12} decreases, approaching r_2 at $Q = \infty$.

Fig. 4*B* shows the spectra of Int 2 in Scheme 4 for ba_3-without-CO (blue, green, and red curves) calculated at the three Q values marked on the curves in Fig. 4*A*; the dashed curves (green and red) represent the fast-slow order of the microscopic rates, while the solid curves (green and red) represent the slow-fast rate combination. The spectrum of compound **A** of the bovine aa_3 is plotted for comparison (black curve). The amplitude of the Int 2 spectrum at $Q_{\min}$ (bold, blue trace) is only a fraction of the model compound **A** bovine spectrum. When the first step (O_2 binding) is slower than the second one (Fig. 4*A*, solid lines), the amplitude of Int 2 increases and approaches that of the model compound **A** spectrum at high values of Q (Fig. 4*B*, solid green and red curves). However, when the first (equilibrium) step is faster than the second (irreversible) step (Fig. 4*A*, dashed lines), the amplitude of Int 2 decreases further at higher Q (Fig. 4*B*, dashed, green and red curves, respectively). These results show unambiguously that only the mechanism with the slow-fast step combination (Scheme 5) produces an acceptable compound **A** spectrum and that the 9.3 μs and not the shorter 4.8 μs lifetime should be assigned to O_2 binding to heme $a_3{}^{2+}$. This assignment is confirmed by the dependence of the apparent lifetimes on the O_2 concentration. At half the O_2 concentration (45 μM), the 9.3-μs lifetime was increased by a factor of two to 18 μs, which is expected if there is no reversibility, while the 4.8-μs lifetime was unaffected (see *SI Text* and Figs. S4 and S5 for details). The 9.3-μs lifetime observed at 90-μM O_2 concentration corresponds to a lifetime of approximately 1 μs at 1 mM O_2 or a second-order rate constant for O_2 binding of 1×10^9 M^{-1} s^{-1}. This rate is 10 times faster than observed in our laboratory for the bovine enzyme in the absence or presence of CO.

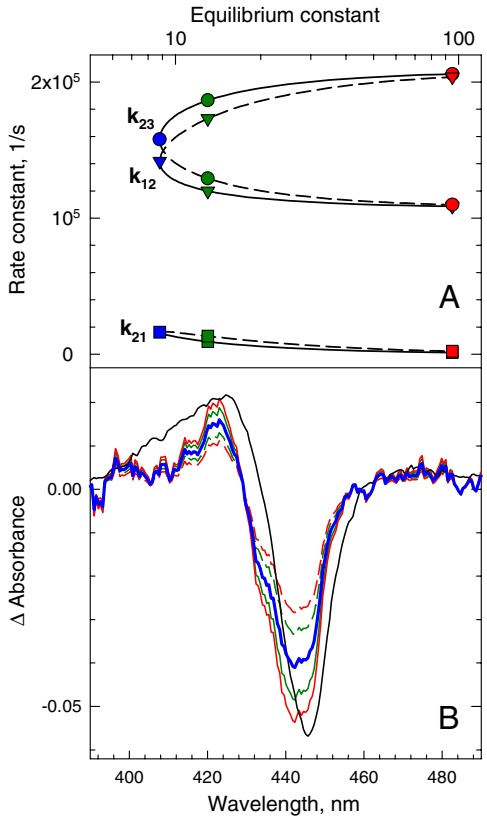

Fig. 4. (*A*) The dependence of the rate constants, k_{12} (triangles), k_{21} (squares), and k_{23} (circles), in Scheme 4 on the equilibrium constant Q above its minimum value (7.8) for the ba_3-without-CO; at any $Q > Q_{min}$ all three microscopic rates have two values (Eqs. **1**, **2**, and **3**). Dashed lines: decreasing k_{23} and increasing k_{12}, approaching r_2 and r_1 at $Q = \infty$, respectively. Solid lines: increasing k_{23} and decreasing k_{12}, approaching r_1 and r_2 at $Q = \infty$, respectively. (*B*) The spectra of Int 2 for ba_3-without-CO calculated at the three Q values marked on the curves in *A*; the bold blue spectrum is at $Q = Q_{min}$, the dashed (green and red) and solid (green and red) curves represent the fast-slow and slow-fast rate combinations, respectively. The spectrum of compound **A** of the bovine aa_3 (CO flow-flash method) is the model spectrum (black curve).

The slow-fast mechanism in Scheme 5 is in contrast to recent fast-mixing CO flow-flash studies on ba_3 (O_2 concentration of approximately 1 mM) in which apparent lifetimes of 5.3 μs and 13 μs were assigned to O_2 binding to heme a_3 and the subsequent formation of $\mathbf{P_R}$, respectively (6). The reduced yield of compound **A** was attributed to the reversibility of O_2 binding based on a model assuming established coupled equilibria (6). This assumption is, however, not valid because at least one of the equilibria, that of CO leaving Cu_B^+, has a reported lifetime of approximately 30 ms (14), more than 1,000 times longer than the measured rate of O_2 binding to heme a_3. However, the reported apparent rates and reduced yield of compound **A** (6) are in agreement with the slow-fast rate combination discussed above, suggesting that the 13 μs lifetime represents O_2 binding to heme a_3 and the 5.3-μs lifetime the subsequent **P** formation accompanied by heme *b* oxidation.

Analysis of the ba_3-With-CO Data Using a Slow-Fast Rate Combination. For ba_3-with-CO, the 110 μs lifetime is assigned to the O_2 binding

$$\mathbf{R} \xrightarrow[O_2]{9.3\ \mu s} \mathbf{A} \xrightarrow{4.8\ \mu s} \mathbf{P_I} \xrightarrow{55\ \mu s} \mathbf{P_{II}} \xrightarrow{1.0\ ms} \mathbf{O}$$

Scheme 5. The slow-fast sequential mechanism for the reaction of ba_3 with photoproduced O_2 in the absence of CO.

based on the following arguments. The spectrum of Int 2 in Scheme 3 for ba_3-with-CO (Fig. 3*B*, red curve) has the same shape as that of intermediate 3 ($\mathbf{P_I}$) in Scheme 2 in the absence of CO (Fig. 3*A*, red curve) but with a significantly smaller amplitude, a situation reminiscent of the smaller-than-expected amplitude of Int 2 (compound **A**) for ba_3-without-CO discussed above. Therefore, we extracted the spectra of the intermediates for ba_3-with-CO using the slow-fast step combination in Scheme 6. Using this mechanism, the spectrum of Int 2 for ba_3-with-CO was found to be in good agreement with that of Int 3 ($\mathbf{P_I}$) for ba_3-without-CO (Fig. S6), showing the 110 μs lifetime should be assigned to O_2 binding.

The 110 μs O_2 binding corresponds to a lifetime of approximately 10 μs at 1 mM O_2, which is practically identical to the 13 μs lifetime (our assignment) observed in the recent fast-mixing CO flow-flash experiment on ba_3 (1 mM O_2) (6). The 110-μs step is followed by a faster process, 59 μs, which is attributed to the subsequent heme *b* rereduction. This rate is very similar to the rate of electron transfer between heme *b* and Cu_A for ba_3-without-CO (55 μs) and in good agreement with the analogous rate recently reported using the CO flow-flash method (7).

Consistent with our results on ba_3-without-CO and the recent fast-mixing CO flow-flash results on ba_3 (6, 7), the heme a_3 in ba_3 is not converted to the 580-nm oxyferryl form (**F**) but rather maintains the spectral characteristics of **P**. This suggests that the proton acceptor proposed to be responsible for the spectral difference between the **P** and **F** forms in the aa_3 enzyme, possibly the cross-linked tyrosine or the hydroxide bound to Cu_B, may be different from that in ba_3 (6, 7). It should also be noted that it is the spectral difference related to heme a_3 that distinguishes the **P** and **F** forms and not their relative positions in the order of the sequential intermediates. Accordingly, we designate the second 610 nm absorbing species in the ba_3 kinetics as a **P** state ($\mathbf{P_{II}}$) regardless of its place in the scheme.

Time-Evolution of the Intermediates. The relative concentration profiles of the intermediates of ba_3 in the absence and presence of CO as a function of time are shown in Fig. 5 (dashed and solid lines, respectively). The time profiles are calculated based on Scheme 5, established for the kinetic description of ba_3-without-CO and supported by the previously reported CO flow-flash experiment (6). For ba_3-with-CO, we have replaced the 9.3-μs O_2 binding in Scheme 5 with the observed 110-μs O_2 binding. The time profiles for ba_3-without-CO show that the 9.3-μs O_2 binding and the subsequent 4.8-μs $\mathbf{P_I}$ formation result in a limited, although observable, accumulation of compound **A** (Fig. 5, dashed green line). When O_2 binding slows down to 110 μs in the ba_3-with-CO reaction, there are potentially two faster steps, the 4.8-μs $\mathbf{P_I}$ formation and the subsequent 55-μs $\mathbf{P_{II}}$ formation. In this case, the predicted accumulation of compound **A** (Fig. 5, solid green curve) is too small to be detected; however, $\mathbf{P_I}$ reaches high enough concentration to be resolved by the exponential fitting (Fig. 5, solid red curve).

The Superfast Steps in the ba_3 O_2 Kinetics. The Effect of CO on O_2 Access to Heme a_3. The above results demonstrate unequivocally that the binding of photoproduced dioxygen to reduced ba_3 in the absence of CO is 10 times faster than the O_2 binding observed in the presence of CO in our double-laser flow-flash experiment and that reported using the CO flow-flash method (6) (our interpretation). These results suggest that the photodissociated CO, either bound to Cu_B^+ and/or trapped at a ligand docking site,

$$\mathbf{R} \xrightarrow[O_2]{110\ \mu s} \mathbf{P_I} \xrightarrow{59\ \mu s} \mathbf{P_{II}} \xrightarrow{0.82\ ms} \mathbf{O}$$

Scheme 6. The slow-fast sequential mechanism for the reaction of ba_3 with photoproduced O_2 in the presence of CO.

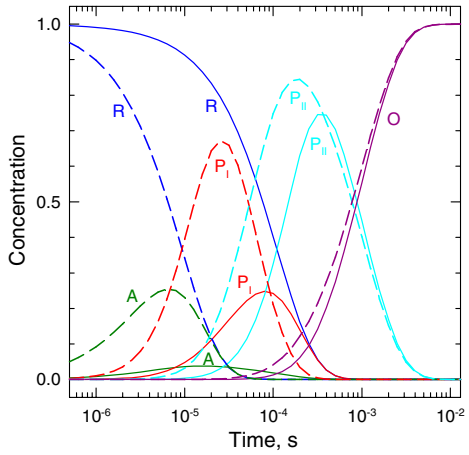

Fig. 5. The time-dependent concentration profiles of the sequential intermediates for the reaction of reduced ba_3 with dioxygen in the absence and presence of CO (broken and solid lines, respectively). The time-dependent concentration profiles in the absence of CO were calculated based on the slow-fast unidirectional sequential model (Scheme 5) with apparent lifetimes of 9.3 μs, 4.8 μs, 55 μs, and 1.0 ms. The time profiles in the presence of CO were calculated based on the same scheme except the 9.3-μs O_2 binding was replaced with the experimental 110-μs lifetime.

impedes access of O_2 to heme a_3 in ba_3. Time-resolved step-scan FTIR studies have suggested that 15–20% of CO may be trapped at a ligand docking site following photolysis of CO from heme $a_3{}^{2+}$ in ba_3 (20). The CO at a site close to Cu_B may interact with the heme methyl group and the propionate side chain of ring A, thus impeding access of O_2 to the binuclear center (20, 21). An alternative explanation for the slower O_2 binding rate in the presence of CO is that the reduced enzyme generated after CO photodissociation has a conformation less favorable for O_2 access to heme a_3 than the normal reduced enzyme.

The other remarkable feature of the O_2 reduction mechanism in ba_3 is the fast $\mathbf{P_I}$ formation and heme b oxidation (approximately 5 μs) in both the absence of CO (this study) and the presence of CO (our assignment) (6). This rate is approximately 10 times faster than the corresponding rate reported for the bovine enzyme (2, 22) and may arise from a shorter distance between heme a_3 and Cu_B in ba_3 (23, 24) or a redox potential difference that favors electron transfer from heme b^{2+} to heme $a_3{}^{2+}$-O_2.

Is Cu_B an Obligatory Stop for O_2 Entry to Heme a_3 in ba_3? The obligatory path of CO to and from heme a_3 in the bovine enzyme has been proposed to involve the binding of CO to $Cu_B{}^+$ (13, 25), and an analogous mechanism has been postulated for ba_3 (14, 26); the O_2 ligand has been proposed to follow the same path (27). However, crystallographic studies using Xe and Kr to map out the O_2 pathway within ba_3 have indicated that there is no straight-access line from Xe1, the site closest to the binuclear cavity, to Cu_B, and that Trp229 and His283 appear to form a barrier that O_2 needs to circumvent to access the dinuclear center (21). These observations, together with the long lifetime of the transient $Cu_B{}^+$-CO complex in ba_3 (14), suggest that Cu_B may not necessarily act as an obligatory stop for O_2 entry to heme a_3 in ba_3-with-CO. In the absence of CO, the entry of O_2 to heme a_3 in ba_3 may or may not involve prior binding to Cu_B.

Possible Implications of CO on Intramolecular Electron Transfer. Whether ba_3 can simultaneously accommodate two ligands at the active site is unclear (28–30). If simultaneous binding of CO to $Cu_B{}^+$ and O_2 to heme $a_3{}^{2+}$ does occur, the CO-bound Cu_B may not be able to act as an electron donor during dioxygen reduction. Because the rate of $\mathbf{P_I}$ formation is the same in the absence of CO (this study) and presence of CO (our assignment) (6), the donor of the fourth electron required for dioxygen bond cleavage would presumably be the same in both cases, perhaps the cross-linked tyrosine (31, 32), as suggested for the reaction of O_2 with the mixed-valence aa_3 enzyme (32). Alternatively, the binding of O_2 to heme $a_3{}^{2+}$ may reduce the affinity of $Cu_B{}^+$ for CO, causing CO to dissociate, thus allowing $Cu_B{}^+$ to act as an electron donor to the bound dioxygen.

Conclusions. Our results demonstrate superfast O_2 binding in ba_3 in the absence of CO and that the presence of CO directly or indirectly impedes dioxygen access to the active site thus making the CO flow-flash method inapplicable. The O_2 binding in ba_3-without-CO is also 10 times faster than its binding to the bovine enzyme under similar conditions. Comparative studies on the bovine enzyme in our laboratory have shown that the presence of CO does not affect the O_2 binding rate. This suggests that O_2 binding in the bovine enzyme and ba_3 are inherently different. Crystallographic studies of Xe binding within the internal cavity of ba_3 show that the dimensions of the ba_3 O_2 channel pose no obstruction for O_2 access to the a_3-Cu_B center (21). In contrast, in *Rhodobacter sphaeroides, Paracoccus denitrificans*, and bovine aa_3 enzymes, there is a constriction point that reduces the channel diameter (21); therefore in these oxidases a conformational change would be required for dioxygen access to the binuclear site. We propose that the structural differences in the dioxygen channel between these two enzymes give rise to the 10-times faster O_2 binding in the ba_3 enzyme. The elevated O_2 transport and cleavage rates may be advantageous to the organism considering the low oxygen solubility under atmospheric pressure at 70 °C, the optimum growth temperature of the *T. thermophilus* HB8. Whether the CO binding to Cu_B interferes with the access of other ligands to the active site, including that of NO, will be determined in due course.

Materials and Methods

Enzyme and O_2-Complex Preparation. The wild-type ba_3 was isolated from *T. thermophilus* HB8 cells according to previously published procedures (5, 33). The fully reduced CO-bound enzyme was generated upon addition of anaerobic solutions of sodium ascorbate and ruthenium (II) hexammine chloride to deoxygenated oxidized enzyme solutions under nitrogen atmosphere, followed by exposure to CO atmosphere. The photolabile O_2 carrier, (μ-peroxo)(μ-hydroxo)bis[bis(bipyridyl)-cobalt (III)] complex, was synthesized as previously described (34).

Time-Resolved Optical Absorption Measurements. The reactions of the reduced ba_3 with O_2 were monitored by time-resolved optical absorption spectroscopy using a CCD detector (Andor Technology). The spectra were recorded between 360–760 nm at delay times from 500 ns to 20 ms after laser photolysis. The enzyme solutions with or without CO were mixed in a 1:1 volume ratio with a solution of the photolabile O_2-carrier. The O_2 was generated upon photolysis with a 355-nm laser pulse (Nd:YAG, 7 ns pulse). In the presence of CO, the reaction was initiated by simultaneously photolyzing the CO-bound enzyme with 532-nm laser light because of the high absorbance of the O_2 carrier at 355 nm. The time-resolved difference spectra were analyzed by SVD and global exponential fitting using Matlab (Mathworks) (15–18). To test the validity of the proposed mechanism, the extracted experimental intermediate spectra were compared to the respective model spectra of the proposed intermediates.

ACKNOWLEDGMENTS. This work was supported by the National Institutes of Health Grants GM53788 (O.E.) and GM 35342 (J.F.) and the Science Foundation Ireland (BICF685 to T.S.).

1. Einarsdóttir Ó (1995) Fast reactions of cytochrome oxidase. *Biochim Biophys Acta* 1229:129–147.
2. Ferguson-Miller S, Babcock GT (1996) Heme/copper terminal oxidases. *Chem Rev* 96:2889–2907.
3. Gibson QH, Greenwood C (1963) Reactions of cytochrome oxidase with oxygen and carbon monoxide. *Biochem J* 86:541–554.
4. Pereira MM, Santana M, Teixeira M (2001) A novel scenario for the evolution of haem-copper oxygen reductases. *Biochim Biophys Acta* 1505:185–208.

5. Giuffrè A, et al. (1999) Kinetic properties of ba_3 oxidase from *Thermus thermophilus*: Effect of temperature. *Biochemistry* 38:1057–1065.
6. Siletsky SA, et al. (2007) Time-resolved single-turnover of ba_3 oxidase from *Thermus thermophilus*. *Biochim Biophys Acta* 1767:1383–1392.
7. Smirnova IA, Zaslavsky D, Fee JA, Gennis RB, Brzezinski P (2008) Electron and proton transfer in the ba_3 oxidase from *Thermus thermophilus*. *J Bioenerg Biomembr* 40:281–287.
8. Hunsicker-Wang LM, Pacoma RL, Chen Y, Fee JA, Stout CD (2005) A novel cryoprotection scheme for enhancing the diffraction of crystals of recombinant cytochrome ba_3 oxidase from *Thermus thermophilus*. *Acta Crystallogr D* 340–343.
9. Soulimane T, et al. (2000) Structure and mechanism of the aberrantba_3-cytochrome *c* oxidase from *Thermus thermophilus*. *EMBO J* 19:1766–1776.
10. Zimmermann BH, Nitche CI, Fee JA, Rusnak F, Münck E (1988) Properties of a copper-containing cytochrome ba_3: A second terminal oxidase from the extreme thermophile *Thermus thermophilus*. *Proc Natl Acad Sci USA* 85:5779–5783.
11. Keightley J, et al. (1995) Molecular genetic and protein chemical characterization of the cytochrome ba_3 from *Thermus thermophilus* HB8. *J Biol Chem* 270:20345–20358.
12. Giuffrè A, et al. (1999) The heme-copper oxidases of *Thermus thermophilus* catalyze the reduction of nitric oxide: Evolutionary implications. *Proc Natl Acad Sci USA* 96:14718–14723.
13. Einarsdóttir Ó, et al. (1993) Photodissociation and recombination of carbonmonoxy cytochrome oxidase: Dynamics from picoseconds to kiloseconds. *Biochemistry* 32:12013–12024.
14. Koutsoupakis K, Stavrakis S, Pinakoulaki E, Soulimane T, Varotsis C (2002) Observation of the equilibrium Cu_B-CO complex and functional implications of the transient heme a_3 propionates in cytochrome ba_3-CO from *Thermus thermophilus* Fourier transform infrared (FTIR) and time-resolved step-scan FTIR studies. *J Biol Chem* 277:32860–32866.
15. Georgiadis KE, Jhon N-I, Einarsdóttir Ó (1994) Time-resolved optical absorption studies of intramolecular electron transfer in cytochrome *c* oxidase. *Biochemistry* 33:9245–9256.
16. Hug SJ, Lewis JW, Einterz CM, Thorgeirsson TE, Kliger DS (1990) Nanosecond photolysis of rhodopsin: Evidence for a new, blue-shifted intermediate. *Biochemistry* 29:1475–1485.
17. Szundi I, Lewis JW, Kliger DS (1997) Deriving reaction mechanisms from kinetic spectroscopy. Application to late rhodopsin intermediates. *Biophys J* 73:688–702.
18. Szundi I, Van Eps N, Einarsdóttir Ó (2003) pH dependence of the reduction of dioxygen to water by cytochrome *c* oxidase. 2. Branched electron transfer pathways linked by proton transfer. *Biochemistry* 42:5074–5090.
19. Einarsdóttir Ó, Szundi I, Van Eps N, Sucheta AS (2002) P_M and P_R forms of cytochrome *c* oxidase have different spectral properties. *J Inorg Biochem* 91:87–93.
20. Koutsoupakis C, Soulimane T, Varotsis C (2003) Ligand binding in a docking site of cytochrome *c* oxidase: A time-resolved step-scan Fourier transform infrared study. *J Am Chem Soc* 125:14728–14732.
21. Luna VM, Chen Y, Fee JA, Stout CD (2008) Crystallographic studies of Xe and Kr binding within the large internal cavity of cytochrome ba_3 from *Thermus thermophilus*: Structural analysis and role of oxygen transport channels in the heme-Cu oxidases. *Biochemistry* 47:4657–4665.
22. Sucheta A, Szundi I, Einarsdóttir Ó (1998) Intermediates in the reaction of fully reduced cytochrome *c* oxidase with dioxygen. *Biochemistry* 37:17905–17914.
23. Than ME, Soulimane T (2001) *Handbook of Metalloproteins* (Wiley, Chichester, UK).
24. Liu B, et al. (2009) Combined microspectrophotometric and crystallographic examination of chemically reduced and X-ray radiation-reduced forms of cytochrome ba_3 oxidase from *Thermus thermophilus*: Structure of the reduced form of the enzyme. *Biochemistry* 48:820–826.
25. Dyer RB, Einarsdóttir Ó, Killough PM, López-Garriga JJ, Woodruff WH (1989) Transient binding of photodissociated CO to Cu_B^+ of eukaryotic cytochrome oxidase at ambient temperature. Direct evidence from time-resolved infrared spectroscopy. *J Am Chem Soc* 111:7657–7659.
26. Woodruff WH, Dyer RB, Einarsdóttir Ó (1993) Spectroscopy, dynamics, and function of cytochrome oxidase. *Biological Spectroscopy, Part B*, eds RJH Clark and RE Hester (Wiley, Chichester, UK), pp 189–233.
27. Blackmore RS, Greenwood C, Gibson QH (1991) Studies of the primary oxygen intermediate in the reaction of fully reduced cytochrome oxidase. *J Biol Chem* 266:19245–19249.
28. Hayashi T, Lin IJ, Chen Y, Fee JA, Moënne-Loccoz P (2007) Fourier transform infrared characterization of a Cu_B-nitrosyl complex in cytochrome ba_3 from *Thermus thermophilus*: Relevance to NO reductase activity in heme-copper terminal oxidases. *J Am Chem Soc* 129:14952–14958.
29. Ohta T, Kitagawa T, Varotsis C (2006) Characterization of a bimetallic-bridging intermediate in the reduction of NO to N_2O: A density functional theory study. *Inorg Chem* 45:3187–90.
30. Pilet E, et al. (2004) NO binding and dynamics in reduced heme-copper oxidases aa_3 from *Paracoccus denitrificans* and ba_3 from *Thermus thermophilus*. *Biochemistry* 43:14118–14127.
31. Offenbacher A, et al. (2009) A spectroscopic investigation of a tridentate Cu-complex mimicking the tyrosine-histidine cross-link of cytochrome *c* oxidase. *J Phys Chem B* 113:7407–7417.
32. Proshlyakov DA, Pressler MA, Babcock GT (1998) Dioxygen activation and bond cleavage by mixed-valence cytochrome *c* oxidase. *Proc Natl Acad Sci USA* 95:8020–8025.
33. Soulimane T, Kiefersauer R, Than ME (2002) *Membrane Protein Purification and Crystallization*, eds C Hunte, G von Jagow, and H Schägger (Elsevier, San Diego).
34. MacArthur R, Sucheta A, Chong FS, Einarsdóttir Ó (1995) Photodissociation of a (μ-peroxo)(μ-hydroxo)bis[bis(bipyridyl)cobalt(III)] complex: A tool to study fast biological reactions involving O_2. *Proc Natl Acad Sci USA* 92:8105–8109.